Inorg. Chem. **2006**, *45*, 3549–3556

Citrate, in Collaboration with a Guanidinium Ion, as a Generator of Cubane-like Complexes with a Range of Metal Cations: Synthesis, Structures, and Magnetic Properties of $[C(NH_2)_3]_8[(M^{II})_4(cit)_4]\cdot 8H_2O$ (M = Mg, Mn, Fe, Co, Ni, and Zn; cit = Citrate)

Timothy A. Hudson,[†] Kevin J. Berry,[‡] Boujemaa Moubaraki,[§] Keith S. Murray,*[,§] and Richard Robson*[,†]

Westernport Secondary College, Hastings, Victoria 3915, Australia, School of Chemistry, University of Melbourne, Parkville, Victoria 3010, Australia, and School of Chemistry, Building 23, Monash University, Wellington Road, Clayton, Victoria 3800, Australia

Received October 14, 2005

Aqueous reaction mixtures containing citric acid, guanidinium carbonate, and a range of metal cations (Mg^{2+}, Mn^{2+}, Fe^{2+}, Co^{2+}, Ni^{2+}, and Zn^{2+}) at room temperature give crystalline products of composition $[C(NH_2)_3]_8[(M^{II})_4(cit)_4]\cdot 8H_2O$ (cit = citrate). In all cases, the crystals are suitable for single-crystal X-ray diffraction studies, which reveal that the compounds are isostructural (space group $P4_2/n$; $a \sim 16.2$ Å, and $c \sim 11.5$ Å). As was intended, cubane-like $[M_4(cit)_4]^{8-}$ complex anions are present. The individual citrate units are chiral, but each cubane unit contains two of one hand and two of the other, related around an S_4 axis. The cubane units are involved in no less than 40 H-bonding interactions with guanidinium cations and lattice water molecules. Detailed susceptibility and magnetization studies show that the intracluster magnetic coupling within the Mn^{II}, Fe^{II}, Co^{II}, and Ni^{II} cubanes is very weak in all cases with J values of –0.82, –0.43, and –0.09 cm^{-1} for the Mn, Fe, and Co species, respectively. A two-J model gave the best agreement with the susceptibility and high-field magnetization data for the Ni^{II} case, over the whole temperature range studied, and the sign of the parameters, $J_{12} = -0.3$ cm^{-1} and $J_{13} = +2.97$ cm^{-1}, correlated with the two Ni–(μ_3-O)–Ni angles observed in the cluster structure. All members of the 3d-block $[M_4(cit)_4]^{8-}$ family have spin ground states, S_T, of zero, with the higher S_T levels just a few reciprocal centimeters away in energy.

Introduction

Cubane-related metal complexes have aroused much interest because of their unusual properties, their potential as single-molecule magnets (SMMs),[1] and their biological relevance, interest considerably intensified recently by the identification of a Mn_3Ca cubane-like core at the active site of photosystem II.[2] It has been proposed that a family of appropriately trisubstituted methoxide ligands, as represented in **I**, in which *X*, *Y*, and *Z* may be a range of N, O, and other donors, may show a strong predisposition to form cubane-like metal complexes.[3] One of the simplest imaginable

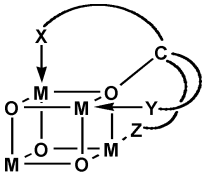

I

members of this family is the tricarboxy-substituted methoxide ion, $^{-}OC(CO_2^{-})_3$, a new oxy anion of carbon, which was recently reported to afford a series of cubane-like metal complexes, as shown in Figure 1.[3] The "short reach" of the

* To whom correspondence should be addressed. E-mail: keith.murray@sci.monash.edu.au (K.S.M.), r.robson@unimelb.edu.au (R.R.).
[†] University of Melbourne.
[‡] Westernport Secondary College.
[§] Monash University.

(1) Mirebeau, I.; Hennion, M.; Casalta, H.; Andres, H.; Güdel, H. U.; Irodova, A. V.; Caneschi, A. *Phys. Rev. Lett.* **1999**, *83*, 628.
(2) Ferreira, K. N.; Iverson, T. M.; Maghlaoui, K.; Barber, J.; Iwata, S. *Science* **2004**, *303* (5665), 1831.
(3) Abrahams, B. F.; Hudson, T. A.; Robson, R. *J. Am. Chem. Soc.* **2004**, *126*, 8624.

10.1021/ic051779m CCC: $33.50
Published on Web 04/06/2006

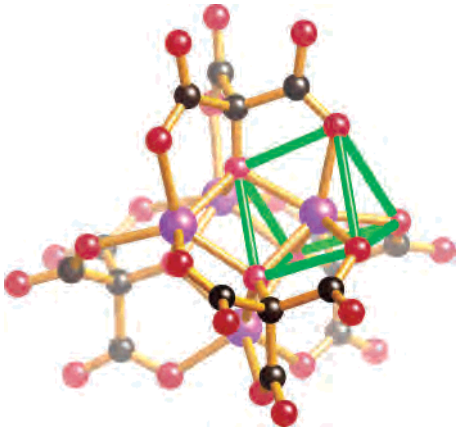

Figure 1. Cubane-like structure of the $M_4(C_4O_7)_4^{8-}$ unit. The trigonal-prismatic coordination geometry of the metal centers is highlighted in green for one of them.

ligand's arms constrains the five-membered chelate rings to be close to planar; consequently, a trigonal-prismatic geometry is imposed upon the metal centers, as can be seen in Figure 1. We speculate that the ligand $(O^-)C(CH_2CO_2^-)_3$, with an additional methylene link in each arm, may also have a strong tendency to impose cubane structures on its metal derivatives, but now the ligand's arms have sufficient "reach", models suggest, to be able to connect to octahedral coordination sites around the metal. Unfortunately, the acid, $HOC(CH_2COOH)_3$, is not readily available, although we plan to synthesize it and study its metal complexes. Citric acid, on the other hand, is very readily available and cheap. Its tetraanion, $^-OC(CO_2^-)(CH_2CO_2^-)_2$, hereafter cit^{4-}, possesses one arm of the type seen in Figure 1 and two longer ones extended by the insertion of a methylene link. We wondered therefore if it might be possible to induce cit^{4-} to furnish a new type of complex of composition $M_4(cit)_4$ and with a cubane-like structure. Crystallographic structural studies of over 150 metal citrate derivatives can be found in the Cambridge Crystallographic Data File. In addition to many mononuclear citrate complexes, numerous metal−citrate clusters of varying nuclearity, including infinite polymers, have been structurally characterized. The synthesis and structure of a Ni_8 citrate cluster was reported by Strouse et al. in 1977.[4] In 1998, Lippard described a derivative of the complex anion, $[Fe_9O(cit)_8(H_2O)_3]^{7-}$.[5] Since then, Güdel has reported a Ni_7,[6] a Ni_{21},[6] two different Ni_8,[7] and, recently, a Co_6 citrate cluster,[8] the latter containing a $M_4(cit)_4$ cubane core of the sort we had earlier anticipated and been deliberately hunting. We present here the results of a synthetic/structural exploration revealing that citrate, acting in concert with the guanidinium cation, $C(NH_2)_3^+$, which we have recently been employing to generate a number of unusual networks,[9] becomes a very specific generator of cubane-like complexes with a range of different metal cations, yielding an isostructural family of crystalline solids containing $M_4(cit)_4$ cubane units, isolated from other metal centers. The availability of this $M_4(cit)_4$ series of compounds ($M = Mn^{2+}$, Fe^{2+}, Co^{2+}, Ni^{2+}, Zn^{2+}, or Mg^{2+}) with a common structure but with varying numbers of unpaired electrons seemed to offer a rare opportunity to study how magnetic coupling within the cubane varied with the d-electron configuration of the metal. The magnetic properties of this series of compounds, reported below, indicate weak coupling, generally antiferromagnetic except for the Ni^{II} example, which is best interpreted as having ferro- and antiferromagnetic coupling parameters, and less dramatic differences between the various metals than we anticipated. None display SMM features.

Experimental Section

Synthesis. Preparation of $[C(NH_2)_3]_8[(M^{II})_4(cit)_4]\cdot 8H_2O$. To a solution of citric acid (1.0 g, 5.2 mmol) in water (50 mL) was added a solution of $M(NO_3)_2$ (5.2 mmol; M = Co, 1.51 g; M = Zn, 1.55 g; M = Ni, 1.51 g; M = Mn, 930 mg; M = Mg, 1.33 g; M = Fe, in which case the SO_4 salt was used, 2.04 g) in water (50 mL) followed by a solution of guanidinium carbonate (3.78 g, 20.8 mmol) in water (50 mL). The crystals, which separated from the solution after it had been standing overnight, were collected, washed with water, and dried at the pump. Yields: M = Co, 1.93 g, 96%; M = Zn, 1.88 g, 92%. The exact procedure above gave yields of 67% for Ni, 62% for Mn, 76% for Fe, and zero for Mg. Simply by using less water (a total of 45 mL rather than 100 mL), the yield of the Ni product was increased to 77% and that of the Mg product to 33%. Anal. Calcd for M = Mn: C, 24.3; H, 5.1; N, 21.2. Found: C, 24.6; H, 4.7; N, 21.5. Calcd for M = Fe: C, 24.1; H, 5.0; N, 21.1. Found: C, 24.2; H, 4.8; N, 21.3. Calcd for M = Co: C, 24.0; H, 5.0; N, 21.0. Found: C, 24.2; H, 4.7; N, 21.0. Calcd for M = Ni: C, 24.0; H, 5.0; N, 21.0. Found: C, 24.4; H, 4.7; N, 21.2. Calcd for M = Zn: C, 23.6; H, 4.9; N, 20.6. Found: C, 23.7; H, 4.6; N, 20.8.

Crystallography. Crystal data and details of the data collection and refinement are summarized in Table 1. The crystal data for all compounds were collected using the ϕ and ω scan technique with a Bruker CCD area detector diffractometer fitted with Mo Kα radiation and a graphite monochromator, operating at 130 K. Structural refinements were performed using the *SHELX97* program,[26] which uses a full-matrix least-squares refinement based on F^2. Absorption corrections were performed using the SADABS program.

Magnetic Properties. Magnetic susceptibility and magnetization measurements were made on polycrystalline samples of mass of ca. 20 mg using a Quantum Design MPMS 5 Squid magnetometer. The Co^{II} and Fe^{II} samples were dispersed in a Vaseline mull in order to prevent torquing of crystallites occurring at low temperatures and high fields in these T ground-state species. The samples were contained in gelatin capsules, which were held in the center of a drinking straw that was attached to the end of the sample rod. Diamagnetic corrections were made for the sample holder in obtaining the gram susceptibility and magnetization and for the ligands, using Pascal's constants, in obtaining the molecular

(4) Strouse, J.; Layten, S. W.; Strouse, C. E. *J. Am. Chem. Soc.* **1977**, *99*, 562.
(5) Bino, A.; Shweky, I.; Cohen, S.; Bauminger, E. R.; Lippard, S. *Inorg. Chem.* **1998**, *37*, 5168.
(6) Murrie, M.; Stoeckli-Evans, H.; Güdel, H. U. *Angew. Chem., Int. Ed.* **2001**, *40*, 1957.
(7) Murrie, M.; Biner, D.; Stoeckli-Evans, H.; Güdel, H. U. *Chem. Commun.* **2003**, 230.
(8) Murrie, M.; Teat, S. J.; Stoeckli-Evans, H.; Güdel, H. U. *Angew. Chem., Int. Ed.* **2003**, *42*, 4653.
(9) Abrahams, B. F.; Hawley, A.; Haywood, M. G.; Hudson, T. A.; Robson, R.; Slizys, D. A. *J. Am. Chem. Soc.* **2004**, *126*, 2894.

Table 1. Crystal Parameters for $[C(NH_2)_3]_8[(M^{II})_4(cit)_4]\cdot 8H_2O$ (M^{II} = Co, Fe, Mg, Mn, Ni, and Zn)

param	Co	Fe	Mg	Mn	Ni	Zn
formula	$C_8H_{20}CoN_6O_9$	$C_8H_{20}FeN_6O_9$	$C_8H_{20}MgN_6O_9$	$C_8H_{20}MnN_6O_9$	$C_8H_{20}N_6NiO_9$	$C_8H_{20}N_6O_9Zn$
fw	403.23	400.15	368.61	399.24	403.01	409.67
cryst syst	tetragonal	tetragonal	tetragonal	tetragonal	tetragonal	tetragonal
space group	$P4_2/n$	$P4_2/n$	$P4_2/n$	$P4_2/n$	$P4_2/n$	$P4_2/n$
T (K)	130	130	130	130	130	130
a (Å)	16.1224(8)	16.2542(8)	16.1405(6)	16.2890(12)	16.0562(8)	16.1337(5)
c (Å)	11.5088(11)	11.5350(10)	11.5809(8)	11.5022(17)	11.6135(12)	11.6460(7)
V (Å^{-3})	2991.5(4)	3047.5(3)	3017.0(3)	3051.9(6)	2994.0(4)	3031.4(2)
Z	8	8	8	8	8	8
d_{calc} (g cm $^{-3}$)	1.791	1.744	1.623	1.738	1.788	1.795
μ (mm^{-1})	1.210	1.051	0.180	0.927	1.359	1.682
R1[a] [$I > 2\sigma(I)$]	0.0579	0.0815	0.0900	0.0862	0.0487	0.0442
wR2[b] [$I > 2\sigma(I)$]	0.1425	0.1990	0.2410	0.1973	0.1307	0.1262

[a] $R1 = \sum||F_o| - |F_c||/\sum|F_o|$. [b] $wR2 = \{\sum[w(F_o^2 - F_c^2)^2]/\sum[w(F_o^2)^2]\}^{1/2}$, $w = 1/[\sigma^2(F_o^2) + (aP)^2 + bP]$ and $P = [(F_o^2) + 2(F_c)^2]/3$.

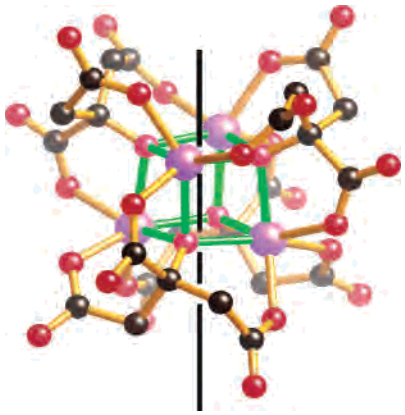

Figure 2. Structure of the $(M^{II})_4(cit)_4^{8-}$ anion (M = Mg, Mn, Fe, Co, Ni, and Zn). The S_4 axis is represented by a black line.

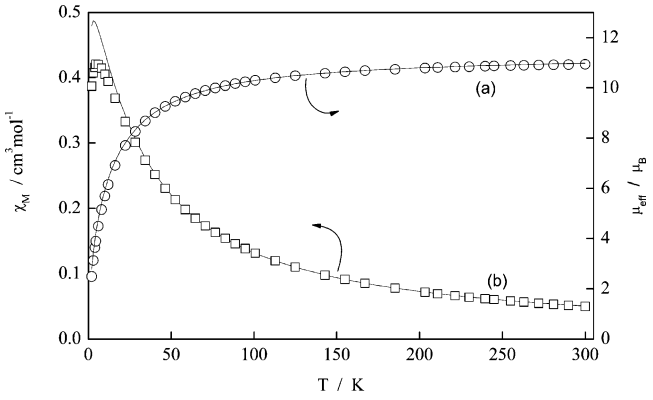

Figure 3. Plots of (a) μ_{eff} and (b) χ_M, per Mn_4, for the cluster $[C(NH_2)_3]_8[Mn_4(cit)_4]\cdot 8H_2O$ in the range of 300−2 K under a field of 1 T. The solid lines are the calculated values for a one-J spin $^5/_2$ model using the best-fit g and J parameters given in the text.

susceptibilities and magnetizations. M values in Nβ units were obtained using the conversion factor 1 Nβ = 5585 cm^3 mol^{-1} Oe.

Results

Synthesis and Structure. When an aqueous solution of guanidinium carbonate is added to an aqueous solution of citric acid containing either Mn^{2+}, Fe^{2+}, Co^{2+}, Ni^{2+}, Zn^{2+}, or Mg^{2+}, the resulting solution, upon standing at room temperature for a few hours, deposits pure, highly crystalline (tetragonal) materials of composition $[C(NH_2)_3]_8[(M^{II})_4(cit)_4]0\cdot 8H_2O$ in good to high yield (except for Mg^{2+}). For all of the metals listed above, the crystals obtained directly from the reaction mixture are suitable for single-crystal X-ray diffraction studies. The structure of the $(M^{II})_4(cit)_4^{8-}$ anion, common to all of these products, is shown in Figure 2.

Magnetic Properties. There are few studies of the magnetic properties of citrate-bridged compounds and of spin−spin coupling across the alkoxo or carboxylato bridges.[6] The magnetic properties of powdered samples of the $[C(NH_2)_3]_8[(M^{II})_4(cit)_4]\cdot 8H_2O$ series, where M^{II} = Mn, Fe, Co, and Ni, are generally indicative of very weak superexchange coupling occurring via the μ_3-alkoxide component of the cubane nucleus, being antiferromagnetic in the Mn, Fe, and Co compounds and ferromagnetic in the Ni compound. A plot of the effective magnetic moment, per Mn_4, vs temperature, measured in a field of 1 T, is shown in Figure 3 for the Mn^{II} cluster. A μ_{eff} value of 11.0 μ_B, for high-spin Mn^{II}, decreases only a little over the range of 300−50 K and then decreases more rapidly to reach 2.5 μ_B at 2 K. The corresponding χ_M (per Mn_4) vs temperature plot shows a maximum at 6 K that is indicative of weak antiferromagnetic coupling. The data were fitted to a single J tetranuclear (cubane, T_d) $-2JS_i\cdot S_j$ model that does not include a zero-field-splitting component, D, which will, in any case, be very small for Mn^{II}.[10] The best-fit parameter values are $g = 1.92$ and $J = -0.82$ cm^{-1}, and this reproduces the μ_{eff} and χ_M data very well, apart from the calculated χ_M values being a little higher than those observed in the χ_M(max) region. The corresponding energy levels have the $S_T = 0$ state (degeneracy 6) as the ground state with a large number of levels very close in energy. These include the following: $S_T = 1$ (15), 1.64 cm^{-1}; $S_T = 2$ (21), 4.92 cm^{-1}; $S_T = 3$ (24), 9.84 cm^{-1}. Any zero-field splitting will cause splitting and removal of the large degeneracies, which, together with the close spacing of the S_T levels and their Zeeman M_S components when in an applied field, make the calculations of the magnetizations, M, very difficult to achieve by use of DS_z^2-type spin Hamiltonians. Tuchagues et al.[10] have previously made such matrix-diagonalization calculations of this large 1296 basis set and plotted the J and D dependencies of μ_{eff}: $\chi_M T$, at a fixed (low) field, for small positive and negative values of J and D. The D values had essentially no effect on the plots, and a cubanoidal macrocyclic alkoxo-

(10) Aussoleil, J.; Cassoux, P.; Tuchagues, J.-P. *Inorg. Chem.* **1989**, *28*, 3051.

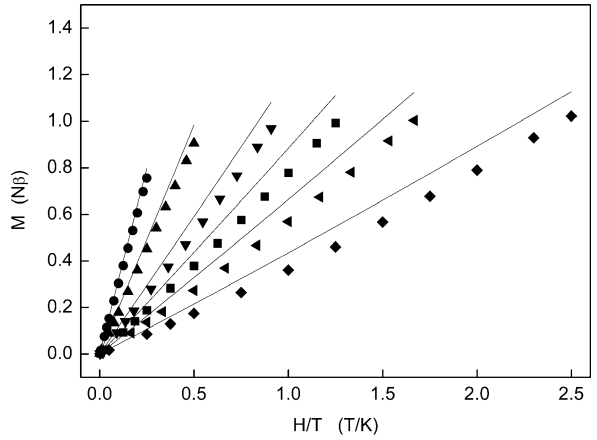

Figure 4. Isothermal plots of reduced magnetization, $M/N\beta$, per Mn^{II}, for $[C(NH_2)_3]_8[Mn_4(cit)_4]\cdot 8H_2O$ measured in fields of between 0 and 5 T and at temperatures 20 K (●), 10 K (▲), 5 K (▼), 4 K (■), 3 K (rotated ▲), and 2 K (◆). The calculated lines using the g and J values given in the text (with $D = 0$) are for temperatures 20−2 K, left to right.

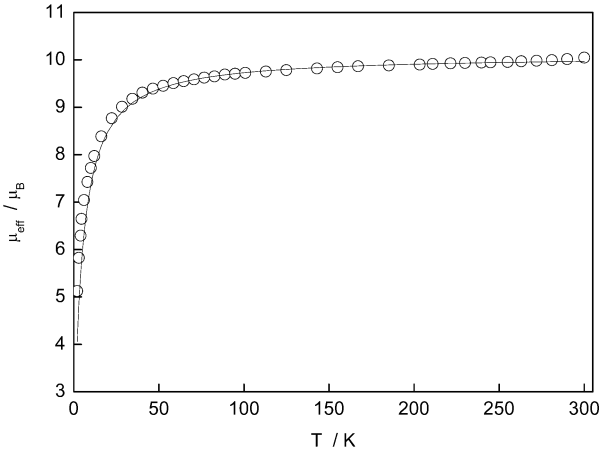

Figure 5. Plot of μ_{eff}, per Fe_4, for the cluster $[C(NH_2)_3]_8[Fe_4(cit)_4]\cdot 8H_2O$ in the range of 300−2 K under a field of 1 T. The solid line shows the calculated values using a one-J spin 2 model and the best-fit g and J parameters given in the text.

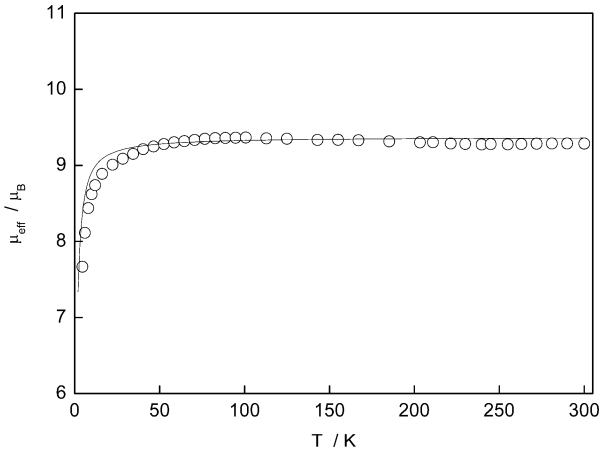

Figure 6. Plot of μ_{eff}, per Co_4, for the cluster $[C(NH_2)_3]_8[Co_4(cit)_4]\cdot 8H_2O$ in the range of 300−2 K under a field of 1 T. The solid line shows the calculated values using a one-J spin $^3/_2$ model and the best-fit g and J parameters given in the text.

bridged Mn^{II} cluster[11] yielded data and fit rather similar to those of the present citrato complex, viz., $g = 1.95$ and $J = -0.51$ cm^{-1}.[10]

The observed magnetization isotherms (2−20 K) for the Mn citrato cubane give a linearlike dependence of M on H, with the largest value of M at 2 K and 5 T being only 1 Nβ, per Mn, behavior again indicative of antiferromagnetic coupling. Interestingly, when the magnetization data are presented as isofield M vs H/T plots, as in Figure 4, when one considers, for example, the top point in each isotherm, "laddering" occurs with unusual broad maxima noted in the $H < 2.5$ T data. Such laddering, when found in Mn^{III} or $Mn^{II/III}$ clusters, is normally indicative of zero-field splitting[12] but can be reasonably well simulated here by use of the $g = 1.92$ and $J = -0.82$ cm^{-1} parameters alone, in conjunction with the tetranuclear spin-coupling model. Alternatively, isothermal plots of M vs H/T are shown in Figure 4, together with the calculated lines, with the latter becoming progressively worse at the lowest temperatures and highest fields because of neglect of weak zero-field splitting, viz., very small D values.

The Fe^{II} complex also contains high-spin, weakly antiferromagnetically coupled Fe^{II} centers, with the μ_{eff} values remaining essentially constant at 10.05 μ_B, per Fe_4, between 300 and ∼100 K and then decreasing rapidly to reach 5.12 μ_B at 2 K (Figure 5). Such behavior is characteristic of distorted six-coordinate Fe^{II} centers having the orbital degeneracy of the $^5T_{2g}$ octahedral states removed,[13] yielding ^{5}A-like ground states, which undergo zero-field splitting and weak antiferromagnetic coupling. Fitting to the single J tetranuclear model[14] for $S = 2$ gave best-fit parameters $g = 2.06$ and $J = -0.43$ cm^{-1} (Figure 5). The energies (degeneracies) of the ground and low-lying S_T states are as follows: $S_T = 0$ (5), 0 cm^{-1}; $S_T = 1$ (12), 0.86 cm^{-1}; $S_T = 2$ (16), 2.58 cm^{-1}; $S_T = 3$ (17), 5.16 cm^{-1}; $S_T = 4$ (15), 8.60 cm^{-1}; ... $S_T = 8$ (1), 30.96 cm^{-1}. Magnetization isotherms, provided in Supporting Information Figure S1, show that the 2−5 K M values come close together in applied fields above ∼3 T and continue to rise steeply. This nonsaturation behavior, combined with the 5-T value of M being ∼1.9 Nβ, per Fe, well below the $S = 2$ M_{sat} of 4 Nβ, is indicative of closely spaced M_S Zeeman levels emanating from zero-field levels that are affected by spin−orbit coupling and antiferromagnetic coupling. Such a situation is extremely difficult to simulate, and we have not achieved this.

The Co^{II} cubane also shows high-spin, essentially uncoupled behavior, with μ_{eff} values, per Co_4, of 9.25 μ_B at 300 K rising a little to reach a broad maximum of 9.35 μ_B at ∼100 K and then decreasing rapidly to reach 7.67 μ_B at 4.2 K (Figure 6). These broad maxima are predicted for $^4T_{1g}$ ground-state Co^{II} systems perturbed by spin−orbit coupling and low-symmetry ligand-field effects.[13,15] The corresponding χ_M^{-1} vs T plot is linear, with a tiny value of the Weiss

(11) (a) McKee, V.; Sheppard, W. B. *Chem. Commun.* **1985**, 158. (b) Brooker, S.; McKee, V.; Sheppard, W. B.; Pannell, L. K. *Dalton Trans.* **1987**, 2555.
(12) Boskovic, C.; Wernsdorfer, W.; Folting, K.; Huffman, J. C.; Hendrickson, D. N.; Christou, G. *Inorg. Chem.* **2002**, *41*, 5107.
(13) Mabbs, F. E.; Machin, D. J. *Magnetism and Transition Metal Complexes*; Chapman and Hall: London, 1973; Chapter 5.
(14) Taft, K. L.; Caneschi, A.; Pence, L. E.; Delfs, C. D.; Papaefthymiou, G. C.; Lippard, S. J. *J. Am. Chem. Soc.* **1993**, *115*, 11753.

constant of −0.5 K. As in the Fe^{II} derivative, this magnetic behavior is consistent with little orbital degeneracy remaining in the single-ion Co^{II} $^4T_{1g}$ parent states. Intracluster spin coupling is extremely weak, as is ground-level zero-field splitting. Fitting to the single-J tetranuclear "spin-only" model yielded a fair fit (Figure 6) of the 300−4 K data using $S = {}^3/_2$, $g = 2.42$, and $J = -0.09$ cm^{-1}, with the high g allowing for spin−orbit coupling. Magnetization isotherms, shown in Figure S2 of the Supporting Information, reveal rather unusual plateaus in the 2−4 K M vs H plots, for $H =$ 1.5−3 T, such that they then follow the same M values above $H = 3$ T and continue increasing above 5 T. The highest value of M at 5 T, per Co, is 1.7 Nβ, which is much reduced from the $S = {}^3/_2$ saturation value, 3 Nβ, because of the spin−orbit coupling effects described above combined with the extremely weak antiferromagnetic coupling. A number of calculations of M vs H were made that included those calculated for a $^4T_{1g}$ state perturbed by spin−orbit coupling[13,15] and those calculated by use of Brillouin functions for an effective spin of $S = {}^1/_2$, with correspondingly high g values, appropriate for the low-temperature regime and moderate strength fields.[8] None of these could reproduce the plateau behavior observed at 2−4 K in fields of 1.5−3 T.

Interestingly, the Ni^{II} cubane appeared to display weak ferromagnetic coupling, as can be seen in Figure 7, which shows the magnetic moments, per Ni_4, remaining constant, at 6.6 μ_B, between 300 and 100 K, then increasing to reach a maximum value of 7.05 μ_B, at 14.4 K, before decreasing rapidly toward 4.7 μ_B at 2 K. Decreases in μ_{eff} of the latter type, at low temperatures, are often ascribed to zero-field splitting of the cluster ground state and/or Zeeman depopulation effects, perhaps influenced by cluster−cluster antiferromagnetic coupling. We show below that they can also be due to intracluster coupling effects using two J values of different sign. Initial attempts to fit the μ_{eff} data excluded the points below 15 K, and a single-J model[10,15] yielded a good fit of the data (Figure 7a) by use of the parameters $g = 2.31$ and $J = +0.51$ cm^{-1}. A small, positive J of this magnitude leads to the $S_T = 4$ ground state being separated from the $S_T = 3$, 2, 1, and 0 levels by 4.08, 7.14, 9.18, and 10.2 cm^{-1}. The kind of magnetic moment plot shown in Figure 7 is often observed in cubane Ni^{II} systems but usually with a steeper increase in moment occurring as the temperature decreases from 300 K because of a correspondingly larger positive J value.[16−19,21]

In attempting to explain the M vs H high-field magnetization data (at temperatures 2−20 K), described below, as well as the decrease noted in μ_{eff} below 15 K (for $H = 1$ T), we began to explore a two-J model, which is actually more appropriate for the S_4 symmetry observed in the citrate cubane structure (vide infra). The Kambe vector coupling model[20] for a two-J situation in Ni^{II} cubanes has been given before.[15−19,21] Figure 7b shows a very good fit to the observed data calculated using the parameters $g = 2.30$, $J_{12} = -0.3$ cm^{-1}, and $J_{13} = +2.97$ cm^{-1} [$J_{12} = J_{23} = J_{34} = J_{41}$ (edges of a distorted Ni_4 tetrahedron); $J_{13} = J_{24}$; $S_{13} = S_1 + S_3$, $S_{24} = S_2 + S_4$, $S_T = S_{13} + S_{24}$]. The energies $E(S_T,S_{13},S_{24})$ of the closely spaced spin states $|S_T, S_{13}, S_{24}\rangle$ are as follows: $|0, 2, 2\rangle$, 0.0 cm^{-1}; $|1, 2, 2\rangle$, 0.60 cm^{-1}; $|2, 2, 2\rangle$, 1.8 cm^{-1}; $|3, 2, 2\rangle$, 3.6 cm^{-1}; $|4, 2, 2\rangle$, 6.0 cm^{-1}; $|1, 1, 2\rangle = |1, 2, 4\rangle =$ 13.68 cm^{-1}; $|2, 1, 2\rangle = |2, 2, 1\rangle = 14.88$ cm^{-1}. Importantly, when these states and energies are introduced into the thermodynamic equation for susceptibility (and μ_{eff})[16] rather than the van Vleck equation, the whole temperature range, down to 2 K, is reproduced for these 1-T data. Thus, we believe that intracluster coupling and Zeeman level (M_S) depopulation effects are more responsible for the low-temperature decrease than are zero-field splitting or cluster−cluster (θ)[21] effects. The two-J model, leading to a $S_T = 0$ ground state, is therefore preferred to the one-J model in

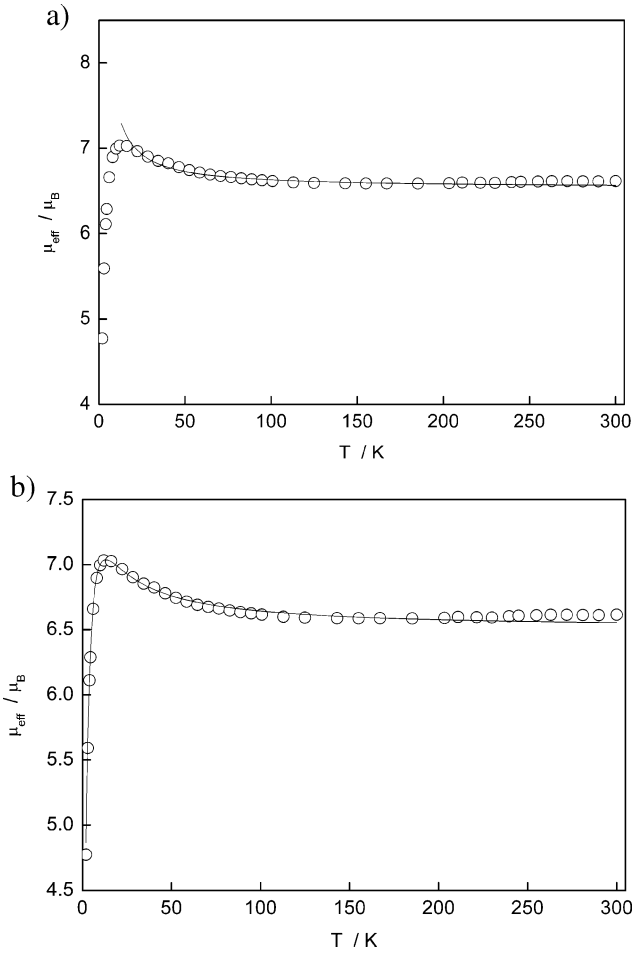

Figure 7. (a) Plot of μ_{eff}, per Ni_4, for the cluster $[C(NH_2)_3]_8[Ni_4(cit)_4]\cdot 8H_2O$ in the range of 300−2 K under a field of 1 T. The solid line shows the calculated values using a one-J spin 1 model and the best-fit g and J parameters given in the text. (b) Experimental data as in part a with the solid line calculated using a two-J spin 1 model and the best-fit parameters of $g = 2.30$, $J_{12} = -0.3$ cm^{-1}, and $J_{13} = +2.97$ cm^{-1}.

(15) Kahn, O. *Molecular Magnetism*; VCH: Weinheim, Germany, 1993; Chapter 3, pp 38−43.
(16) Murray, K. S. *Adv. Inorg. Chem.* **1995**, *43*, 261.
(17) Sieber, A.; Boskovic, C.; Bircher, R.; Waldmann, O.; Ochsenbein, S. T.; Chaboussant, G.; Güdel, H. U.; Kirchner, N.; van Slageren, J.; Wernsdorfer, W.; Neels, A.; Stoeckli-Evans, H.; Janssen, S.; Juranyi, F.; Mutka, H. *Inorg. Chem.* **2005**, *44*, 4315.
(18) Bertrand, J. A.; Ginsberg, A. P.; Kaplan, R. I.; Kirkwood, C. E.; Martin, R. L.; Sherwood, R. C. *Inorg. Chem.* **1970**, *10*, 240.
(19) Aromi, G.; Batsanov, A. S.; Christian, P.; Heliwell, M.; Roubeau, O.; Timco, G. A.; Winpenny, R. E. P. *Dalton Trans.* **2003**, 4466.
(20) Kambe, K. *J. Phys. Soc. Jpn.* **1950**, *5*, 48.
(21) Halcrow, M. A.; Sun, J.-S.; Huffmann, J. C.; Christou, G. *Inorg. Chem.* **1995**, *34*, 4167.

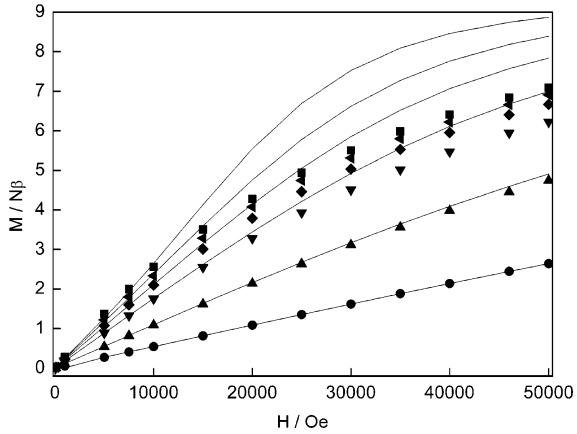

Figure 8. Isothermal plots of reduced magnetization, $M/N\beta$, per Ni^{II}_4, for $[C(NH_2)_3]_8[Ni_4(cit)_4]\cdot 8H_2O$ measured between 2 and 20 K in fields of 0−5 T. The solid lines were calculated using $g = 2.30$, $J_{12} = -0.3$ cm^{-1}, and $J_{13} = +2.97$ cm^{-1} for temperatures 2 (top), 3, 4, 5.5, 10, and 20 K (bottom).

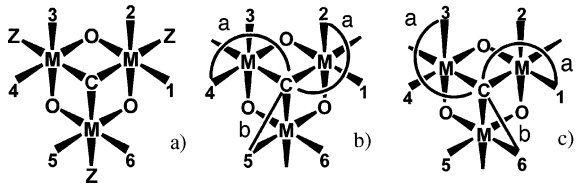

Figure 9. (a) Representations of three faces of a cubane core, viewed along the alkoxide CO bond of one of the ligands, which is located here in the foreground and represented by the central C. The alkoxide O center forming a corner of the cubane is obscured by the C in the figure. The octahedral metal coordination sites external to the cubane are indicated. (b and c) Representations of the two enantiomeric modes of attachment of the citrate ligand. Each cubane unit contains two citrate components of one hand and two of the other hand.

the nickel(II) citrate case. A similar conclusion has recently been reached for a nickel(II) 8-hydroxyquinaldinate cubane complex.[19]

The variable-field magnetization isotherms for the nickel(II) citrate cubane show a very gradual increase in M as H is increased to 5 T, which does not achieve saturation even at 2 K, having a value, per Ni_4, of 7.0 Nβ (1.75 Nβ per Ni), significantly lower than the $S = 1$ M_{sat} value of 2.0 per Ni (Figure 8). This behavior is indicative of spin−orbit coupling affecting the $^3A_{2g}$ single-ion states together with close spacing of the Zeeman M_S levels derived from the closely spaced S_T states, discussed above. It can be seen in Figure 8 that the M values calculated using $g = 2.30$, $J_{12} = -0.3$ cm^{-1}, and $J_{13} = +2.97$ cm^{-1} fit well above 10 K but overestimate the observed values below 10 K, in fields greater than 1 T, probably because of neglect of zero-field splitting in the $S_T = 1-4$ levels lying close above the $S_T = 0$ ground-state level.

Discussion

The structure of the $(M^{II})_4(cit)_4^{8-}$ anion, common to all of the $[C(NH_2)_3]_8[(M^{II})_4(cit)_4]\cdot 8H_2O$ products, is shown in Figure 2. Figure 9a is a schematic representation of the three "visible" faces of a cubane unit viewed along the alkoxide C−O bond of a citrate ligand, which is represented here in the foreground by a C at the center of the figure (with the alkoxide O corner of the cubane being "hidden" behind the C in this view). The three adjacent metal centers have available three extra-cubane octahedral sites, but those labeled Z in Figure 9a are too distant to be accessible to the ligand in question. This, nevertheless, leaves the flexible ligand with multiple ways of choosing three sites out of the six available. Because the individual citrate units have arms of two sorts, numerous isomers, in principle, become possible in a molecule containing four of them. We label the two $-CH_2-CO_2^-$ arms a and the single $-CO_2^-$ arm b. In the $M_4(C_4O_7)_4^{8-}$ cubane unit seen in Figure 1, all of the ligand arms are of type b and are too short to reach the octahedral sites labeled 1−6 in Figure 9a; they therefore impose a trigonal-prismatic geometry on the metal centers, and the resulting molecule is highly symmetrical (local symmetry T_d). In contrast, in the observed structure of $M_4(cit)_4^{8-}$, the two longer a-type arms are, as anticipated, able to access octahedral sites, as can be seen in Figure 2, but they adopt a spiraling character, represented in parts b and c of Figure 9, which imparts chirality to the individual citrate units. If the two a-type arms are attached to sites 2 and 4, as in the enantiomer represented in Figure 9b, there is a natural tendency for the shorter arm, of type b, to attach to site 5 rather than site 6. Likewise, if the spiraling type a arms attach to sites 1 and 3, as is seen Figure 9c, the short b-type arm then is disposed to attach to site 6 rather than site 5. Both enantiomeric forms of the citrate ligand seen in parts b and c of Figure 9 are present in equal numbers in any $M_4(cit)_4^{8-}$ unit. Passing through the $M_4(cit)_4^{8-}$ unit is a 2-fold axis, oriented vertically in Figure 2, and at the center of the cubane is a bar 4 site; in other words, an S_4 axis (vertical in Figure 2) passes through the center of the molecule. Thus, the two upper citrate units, as viewed in Figure 2, are of one hand, related by the 2-fold axis, and the two lower citrate units are of the other hand. The upper and lower pairs are related by the S_4 operation. Associated with the four edges of the cubane that are approximately parallel with the S_4 axis are found the five-membered chelate rings involving the b-type arms. We have seen that constraints in the five-membered chelate rings involving the shorter b-type arms impose trigonal-prismatic geometry on the metal centers in $M_4(C_4O_7)_4^{8-}$. In $M_4(cit)_4^{8-}$, each metal is associated with an a-type arm from two separate citrate ligands and a b-type arm from a third. Thus, similar constraints imposed by the short b-type arms lead to a coordination geometry intermediate between octahedral and trigonal-prismatic. In the recently reported compound[8] $(NMe_4)_3Na[Co_6(cit)_4(H_2O)_{10}]\cdot 11H_2O$, the $Co_4(cit)_4$ component of the Co_6 molecule had an arrangement of citrate ligands very similar to that seen in all six of the products reported in this paper.

The $M_4(cit)_4^{8-}$ anions are bound in the crystal lattice by a very complex system of H bonds, represented in Figure 10, to guanidinium cations, of which there are two types, and to lattice water molecules, which are also H-bonded to guanidinium cations. Half the water molecules are well-defined, and these are shown in Figure 10; the other half, not shown in Figure 10, occupy cavities between cubane units within the columns of cubane units that stack along the z direction and are disordered over four sites, related around a bar 4 site located at the center of the cavity. As shown in Figure

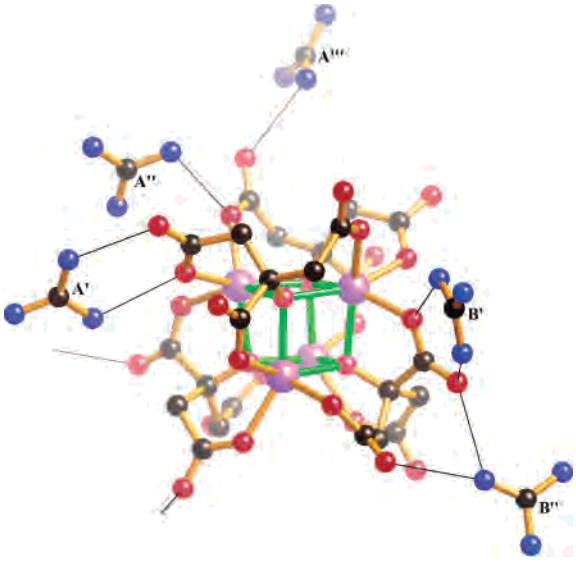

Figure 10. Representation of one-quarter of the H bonds (black lines) between an $(M^{II})_4(cit)_4^{8-}$ anion and either guanidinium cations (two crystallographic types, A and B) or the well-defined water molecules (open circles). The disordered water molecules are not shown. For each one of the H bonds shown here, there are three others not shown that are related to the first by the S_4 operation.

10, each cubane-like anion is involved in no less than 40 H bonds, setting aside those involving the disordered water molecules (O···O, 2.7−2.8 Å; N···O, 2.7−2.9 Å). For clarity, only a quarter of the H bonds are shown in Figure 10, with each one shown generating three others by the S_4 operation.

Analyses of the magnetic susceptibility and magnetization data for the anionic citrato-bridged cubanes show that very weak antiferromagnetic coupling (J range of −0.09 to −0.82 cm^{-1}) is occurring in all cases except for the Ni^{II} compound, which exhibits both ferromagnetic and weak antiferromagnetic coupling pathways. Zero-field splitting of similar or lower size than the J values might also be present, but the large number of closely spaced S_T levels makes it extremely difficult, as discussed in the Mn^{II} and Ni^{II} cases, to extract D values from the magnetization vs field data obtained at low temperatures. This is an important point to note because it is easy to incorrectly assign ground-state S_T and D values from reduced magnetization plots for such situations. A comparison of the J value for $[Ni_4(cit)_4]^{8-}$ to those of other Ni^{II} alkoxo-bridged cubanes shows that compounds of the well-studied type $[Ni_4(chelate)_4(\mu_3\text{-}OR)_4(ROH)_4]$,[16−19,21] where chelate = salicylaldehydato or β-diketonato, have J values in the range of 4−7 cm^{-1} (and even bigger positive J values in the two-J, distorted cubane cases[21]), with energy separations between the $S_T = 4$ ground and upper levels much bigger than those for the citrate cubane, e.g., >32 cm^{-1} to the $S_T = 3$ level. Thus, D can be obtained from the high-field/low-temperature magnetization isotherms and is negative in some cases (vide infra). Mention has been made earlier to a 8-hydroxyquinaldinate case having a $S_T = 0$ ground-state level, but no magnetization data or D values were presented in that case.[19] A similar (relatively) large D situation pertains to some tridentate Schiff base $[Fe_4(sae)_4(MeOH)_4]$ [sae^{2-} = *N*-(ethanolato)salicylaldiminato dianion] and $[Fe_4(chelate)_4(\mu_3\text{-}OR)_4(ROH)_4]$[14] analogues having $S_T = 8$ ground states.

One of the intriguing questions arising from the present study is why the J values are so small in general, being close to zero in the Co^{II} case, and why, for example, the J is negative for $[Fe_4(cit)_4]^{8-}$ while it is positive, ∼+1 cm^{-1}, for $[Fe_4(sae)_4(MeOH)_4]$.[20] For answers, we turn to the coordination and bridging geometries. In the structural section, we saw that the μ_3-O bridging oxygens and the M^{II} atoms were all structurally equivalent in the cubane moiety. This is not (always) the case in the above-mentioned {O, O} chelate or Schiff-base examples because H bonding can, for example, occur across some of the faces of those cubanes.[17,21] The six M−O distances are very similar in the present compounds, and the geometry around the M^{II} ions is intermediate between octahedral and trigonal-prismatic. This contrasts with the tetragonally distorted octahedral geometries in the alkoxo-bridged systems.[17,21,22] These coordination geometry differences will influence which metal "magnetic orbitals" are involved in bridging to the μ_3-O atoms, as well as the efficacy of superexchange overlap, and hence will influence the resulting J values. Taking the Fe^{II} species as examples, the Fe−O distances in $[Fe_4(cit)_4]^{8-}$ are all ∼2.14 Å, while they have two ranges in the axially elongated $[Fe_4(sae)_4(MeOH)_4]$, ∼2.1 and 2.25 Å.[22] The Fe−(μ_3-O)−Fe angles are 96−98° in $[Fe_4(cit)_4]^{8-}$ and 93−104° in $[Fe_4(sae)_4(MeOH)_4]$, with the angles below ∼98° normally leading to a ferromagnetic coupling.[16,17,21] The tetragonal z axis in the sae species is mutually orthogonal to the neighboring Fe^{II} atoms around the cubane, leading to ferromagnetic coupling and a $S_T = 8$ ground state, but this is not the case in the citrate compound.

Similar geometric differences occur in the Ni^{II} examples,[17−19,21] leading to a much weaker, net ferromagnetic coupling in the present cluster. Indeed, the two-J model, with both positive and negative J values and a $S_T = 0$ ground state, describes the magnetic data very well. The structural correlation relating the sign of J to the Ni−(μ_3-O)−Ni angles[17,19,21] also applies, sensitively, to the present cube, with the 96.98(8)° angle correlating with J_{13} and the 99.7(av)° angle correlating with J_{24}. The distorted trigonal-prismatic geometry in the nickel(II) [and cobalt(II) and iron(II)] citrate species might also lead to metal d_{xz} and d_{yz} orbitals being involved in poorer overlap with μ_3-O oxygen atom p orbitals than is the case with d_{z^2} and $d_{x^2-y^2}$ orbitals in the tetragonally distorted octahedral examples.

These geometric differences also influence the magnetic anisotropy of the constituent M^{II} ions and, hence, the anisotropy of the cube. Together with the spin ground state, they also influence the sign and size of the zero-field-splitting parameter, D, for both the M^{II} ion and the cuboidal molecule. Oshio and Nakano[23] have recently discussed these features with regard to designing the very important property of SMM, a property that requires a high-spin ground state and a negative D for the cluster.[24,25] The $[Fe_4(sae)_4(MeOH)_4]$

(22) Oshio, H.; Hoshino, N.; Ito, T.; Nakano, M. *J. Am. Chem. Soc.* **2004**, *126*, 8805.
(23) Oshio, H.; Nakano, M. *Chem.—Eur. J.* **2005**, *11*, 5178.

cluster, for example, has a positive $D_{Fe^{II}}$ value related to the nature of the tetragonally distorted Fe^{II} geometry but a negative D_{mol} value arising from an orthogonal alignment of the four hard-axis Fe^{II} ions. SMM behavior was, consequently, noted with an energy barrier between up and down spins of 28 K.[22,23] In the sap^{2-}(*N*-propanolato) analogue, however, with subtly different tetragonal distortions around the Fe^{II} centers, a collinear easy-axis ($D_{Fe^{II}}$ negative) alignment occurred, D_{mol} was positive, and SMM behavior did not, therefore, occur.[22]

In the present $[M_4(citrate)_4]^{8-}$ clusters, all of the prerequisites for SMM behavior are, unfortunately, absent presumably because the M^{II} coordination and cube geometries are too symmetrical. Except for the Ni^{II} species, the *J* values are small and negative and the spin ground states are zero. The Ni^{II} compound also has a spin-zero ground state arising from positive and negative *J* values. The *D* values for the constituent Ni^{II} and other M^{II} ions and for the corresponding cubane molecules, while not obtained quantitatively here because of the problems associated with the close spacing of the S_T levels, are likely to be close to zero.

These conclusions beg the question as to why SMM behavior was recently claimed in a hexanuclear cobalt(II) citrato cluster, $\{Co_4(cit)_4[Co(H_2O)_5]_2\}^{4-}$, which contains two $Co(H_2O)_5^{2+}$ groups linked on each side of a $Co_4(cit)_4$ cube structurally identical with the present, via anti−syn carboxylato bridges.[8] In our view, this must arise from the anisotropy and negative *D* of the whole hexanuclear cluster, even though the authors conclude that the cluster does not have axial symmetry. No *D* or *J* values were reported. *M* values per Co_6, observed in 5-T fields, at 1.8 K, were 11.2 Nβ for a $11H_2O$ hydrate and 9.0 Nβ for a $7H_2O$ hydrate. The *M* values did not reach saturation in either case and were interpreted as being due to an effective S_T ground state of 3, assuming that in the low-temperature/high-field regime each Co^{II} behaved as a $S_{eff} = {}^1/_2$ center, with $g > 3$. This seems to be a reasonable approximation, but the quantitative calculations of *M* vs *H* data for pseudooctahedral Co^{II} geometries remain a challenge whether in monomers, cubane clusters, or more extended systems. Recently reported calculations are improving the situation markedly.[27,28] Finally, we note that the Co^{II} cubane $[Co_4(hmp)_4(MeOH)_4Cl_4]$ has displayed SMM behavior.[29]

Concluding Remarks

In summary, we report that the cit^{4-} ligand, when it acts in concert with the guanidinium cation, shows remarkable specificity in forming crystalline compounds containing $M_4(cit)_4^{8-}$ cubane-like complex anions with a wide range of divalent cations, M. We note that this chemistry is ideally suited to student laboratory experiments: the reactions are conducted in an aqueous solution, using cheap, nontoxic reagents; with all of the metal cations except Mg^{2+}, they reliably afford high yields of pure, crystalline products and they demonstrate the specific assembly of a complex product of considerable structural interest that can be used to illustrate aspects of symmetry. The magnetic coupling within the Mn^{II}, Fe^{II}, Co^{II}, and Ni^{II} cubanes is very weak in all cases, resulting from both ferromagnetic and antiferromagnetic M−O−M pathways in the Ni compound but from dominant antiferromagnetic pathways in the others. The spin ground state is $S_T = 0$ in all cases, and higher lying S_T states are very close in energy. Electron spin resonance studies on powder and frozen solution samples, at varying (low) temperatures, fields, and frequencies would be worthwhile techniques to employ in the future to gain confirmation of the energy levels derived from magnetism, as well as to indicate the presence of any intercluster interactions.

Acknowledgment. This work was supported by Australian Research Council grants to R.R. and K.S.M.

Supporting Information Available: Figure S1 (magnetization data for $[C(NH_2)_3]_8[Fe_4(cit)_4]\cdot 8H_2O$), Figure S2 (magnetization data for $[C(NH_2)_3]_8[Co_4(cit)_4]0.8H_2O$), and crystallographic information supplied in CIF format. This material is available free of charge via the Internet at http://pubs.acs.org.

IC051779M

(24) Christou, G.; Gatteschi, D.; Hendrickson, D. N.; Sessoli, R. *MRS Bull.* **2000**, *25*, 66.
(25) (a) Gatteschi, D.; Sessoli, R. *Angew. Chem., Int. Ed.* **2003**, *42*, 268. (b) Gatteschi, D.; Sessoli, R.; Cornia, A. In *Comprehensive Coordination Chemistry II*; McCleverty, J. A., Meyer, T. J., Fujita, M., Powell, A., Creutz, C., Eds.; Elsevier: New York, 2004; Vol. 7, Chapter 7.13, pp 779−812.
(26) Sheldrick, G. M. *SHELX97, Programs for Crystal Structure Analysis*; Institüt für Anorganische Chemie der Universität: Göttingen, Germany, 1998.
(27) Palii, A. V.; Tsukerblat, B. S.; Coronado, E.; Clemente-Juan, J. M.; Borrás-Almenar, J. J. *J. Chem. Phys.* **2003**, *118*, 5566−5581.
(28) Boèa, R. *Struct. Bonding* **2006**, *117*, 1.
(29) Yang, E.-C.; Hendrickson, D. N.; Wernsdorfer, W.; Nakano, M.; Zakharov, L. N.; Sommer, R. D.; Rheingold, A. L.; Ledezma-Gairaud, M.; Christou, G. *J. Appl. Phys.* **2002**, *91*, 7382.